Al-Khwarizmi Engineering Journal
ISSN (printed): 1818 – 1171, ISSN (online): 2312 – 0789
Vol. 21, No. 1, March (2025), pp. 89-99

Al-Khwarizmi Engineering Journal

Path Loss Models for 5G Wireless Communication System Using mm wave Communication Channel

Zinah O. Dawood
Department of Information and Communication Engineering, AL-Khwarizmi Engineering College, University of Baghdad, Baghdad, Iraq
Email: zina_osama@kecbu.uobaghdad.edu.iq

(Received 24 December 2023; Revised 23 April 2024; Accepted 5 June 2024; Published 1 March 2025)
https://doi.org/10.22153/kej.2025.06.001

Abstract

Multiple-input multiple-output (MIMO) antenna topologies in wireless communication systems can increase channel capacity and dependability. The use of millimeter (mm)-wave frequency bands in conjunction with other technologies is a substantial step in achieving high data rates for sophisticated AI and multimedia devices. However, transmitting mm wave frequency signals presents challenges such as fading, time delay, propagation and scattering loss. Therefore, optimising propagation parameters is critical to improving performance. This paper examines the influence models for path loss (PL): ABG and CI on the design and analysis of a 4×4 MIMO W-OFDM system employing 16-QAM modulation technique for 5G wireless communication. This paper examines the system using the CI and ABG PL models to assess PL in dB, normal distribution and standard deviation. This paper uses 16-QAM digital modulation, and the simulation results show that the CI PL model-based MIMO W-OFDM system is very robust and successful in signal recovery.

Keywords: *MIMO; millimeter wave; path loss; ABG model; two-parameter CI model*

1. Introduction

The increasing need for wide availability of data and improved mobile data speeds has led to a decrease in the available spectrum within the conventional frequency bands utilised for wireless communication, that is, a frequency lower than 6 GHz. Fifth-generation (5G) wireless communications are being developed as a result of technological innovations such as multiple-input multiple-output (MIMO) [1],[2] and new millimeter-wave (mm wave) frequency band spectrum allocations [3]. These techniques are useful for dealing with the current spectrum shortage [4]. To ensure the accurate, dependable construction of 5G systems, possessing a comprehensive comprehension about the parameters of the propagation channel encompassing microwave and mm wave frequencies is necessary. Revolutionary technologies are predicted to be used by developing 5G communication systems [5]. Developing dependable channel models is important to support engineers in the design because of new possible spectra and innovative architectural concepts [6-8]. Various researchers have already analysed channel characterisation in the mm wave and centimeter (cm)-wave bands [9], [10]. performed modelling and measurements of outdoor propagation in the 60-GHz frequency band in different city streets [11-14]. In recent years, several efforts focused on the examination of mm wave channels, including measurement campaigns, prototype implementations and modelling advancements. According to information theory, three main solutions may be used to enhance system capacity remarkably and meet the design objectives of 5G. Ultradense networks refer to a network architecture characterised by a much higher density of base stations (BS). The use of small-cell technology, commonly referred to as network densification, has already been included into 4G wireless cellular

networks. Increasing the density of a network can enhance its capacity [15-17]. Large amounts of additional bandwidth will be made available to support higher throughput transmission as a result of the migration to higher frequencies [18]. A particularly promising candidate could be mm wave; carrier frequencies range from 30 GHz to 300 GHz. A high spectrum efficiency can be achieved: By completely making use of the space resources, massive MIMO is a technology that utilises a high number of antennas on the transmitter and receiver to increase the accuracy of wireless communication systems. MIMO technology can substantially enhance spectrum efficiency through the use of a considerable quantity of antennas that often number 100 or more. [19]. Each of these technologies will increase the throughput of wireless networks by an order of magnitude or more compared with the current generation of 4G systems. Each of these three solutions exhibit a symbiotic convergence in several aspects: Reduced cell sizes are advantageous in the context of mm wave communications at short distances, whilst the substantial antenna gains facilitated by massive MIMO systems are beneficial in mitigating the substantial signal attenuation experienced by mm wave transmissions. The short wavelength of mm wave frequencies makes them appealing for massive MIMO because the actual dimension of the antenna array may be greatly decreased. If a method to use each of these technologies exists, the 1000-fold increase in 5G capacity can be achieved. The existing mm wave technology raises the operating frequency toa the mm wave band whilst utilising the fundamental design principles of MIMO technology. This paper contributes to the enhancement of the core design concepts of MIMO technology and the use of the mm wave band for operation. The integration of mm wave frequencies partly mitigates the substantial signal attenuation associated with these frequencies and hence enables the establishment of practical minute cell sizes within coverage spans spanning 100 m. This approach not only brings the system closer to achieving a substantial increase in the MIMO gain but also mitigates the substantial signal attenuation seen at mm wave frequencies and hence facilitates the implementation of feasible small cell sizes [14].

1.1.Channel Models Underlying (single_input, single_output, SISO, MIMO)

Wireless channels are classified as large- and small-scale propagation effects (large- and small-scale fading, respectively). Path loss (PL) and shadowing effects caused by great distances are the major causes of large-scale fading. By contrast, short-range fluctuations such as positive and negative interferences from various pathways cause small-scale fading.

1.2. MIMO system

MIMO technology may improve system capacity without increasing bandwidth or broadcast power by increasing the number of transmitting and receiving antennas. The transmitter antenna N and the reception antenna M can gather the signal given by the [1].

$$Y=Hx+n, \quad \ldots(1)$$

where y is the received signal, and H is a matrix is used to deal with transmitted signal x and noise n over the whole channel. Assuming equal Rayleigh channel matrices and average power allocation, the MIMO system's capacity may be expressed in the equation for capacity given by [15].

$$C = \sum_{i=1}^{M} B_i \log_2 \left(\det \left[\boldsymbol{I}_N + \frac{P_{t_i}}{M\sigma_n^2} \boldsymbol{H}\boldsymbol{H}^H \right] \right) = \sum_{i=1}^{M} B_i \log_2 \left(\det \left[\boldsymbol{I}_N + \frac{\rho}{M} \boldsymbol{H}\boldsymbol{H}^H \right] \right), \quad \ldots (2)$$

where the sent signal x, where Bi, det, IN. The first parameter to be determined is the bandwidth allocated to each user. Next, the determinant of the given matrix needs to be calculated. In conclusion, determining the identity of the matrix represented by M and N is necessary. In addition, the average signal-to-noise ratio (SNR) is shown for each channel. When referring to the conjugate transpose of a matrix H, the abbreviation 'HH' is often used as a symbol. The channel matrix can be subdivided into smaller components.

The equation of the matrix used to deal with transmitted signal is given by [15].

$$\boldsymbol{H} = \begin{bmatrix} h_{1,1} & h_{1,2} & \ldots & h_{1,N} \\ h_{2,1} & h_{2,2} & \ldots & h_{2,N} \\ \ldots & \ldots & \ddots & \ldots \\ h_{M,1} & h_{M,2} & \ldots & h_{M,N} \end{bmatrix} \quad \ldots (3)$$

As previously shown, each individual component of the Rayleigh channel matrix may be interpreted as follows by [16]:

$$h_{i,j} = \alpha + j\beta = \sqrt{\alpha^2 + \beta^2} e^{j \arctan \frac{\beta}{\alpha}} = |h_{i,j}| e^{j\phi_{i,j}} \ldots (4)$$

where α,β is a Rayleigh distributed random variable, and |h (i,j) |are random distributed variables. The expression of h (i,j) may be expressed below. The Rayleigh channels are the independent and identically distributed complex zero mean and unit entries; the equation for the capacity is given by [16].

$$h_{i,j} = \text{Normal}\left(0, \frac{1}{\sqrt{2}}\right) + j\text{Normal}\left(0, \frac{1}{\sqrt{2}}\right) \quad \ldots(5)$$

where the normal distribution is generated by Normal. As a result, h (i,j) conforms to the x_2^2 distribution using two degrees of freedom that E= $[h_{i,j}] = 1$.

Because the eigenvalue of $I_N + \frac{p}{m} HH^H$ is produced by the determination equation, the capacity can be calculated by primarily using the eigenvalue of HH^H considering the eigenvalues of the two matrices :

$\{Ap \times q, Bq \times p, p \leq q\}$ eigenvalue of are $AB_{P\times P}$ and$BA_{q\times q}$ equal.

Because a zero eigenvalue does not contribute to the capacity effect, the eigenvalues of HH^H and H^HH are the same, and $\lambda = \lambda_1, \lambda_{2,\ldots\ldots}, \lambda_{\min(N,M)}$ provides the nonzero eigenvalues of the B. The equation for the capacity is given by [16].

$$B = \begin{cases} HH^{II}, M < N, \\ H^H H, M > N. \end{cases} \quad \ldots(6)$$

The MIMO capacity in this case may be expressed as follows:

$$C = \sum_{i=1}^{M} B_i \log_2 \left(\det\left[\mathbf{I}_N + \frac{\rho}{M}\mathbf{H}\mathbf{H}^H\right]\right)$$
$$= \sum_{i=1}^{M} B_i \log_2 \left(\prod_{i=1}^{\min(N,M)} \left[1 + \frac{\rho}{M}\lambda_i^2\right]\right) \quad \ldots(7)$$

MIMO capacity analysis frequently employs singular value decomposition (SVD). The channel matrix in SVD is broken down by the following:

$$H = UDV^H \quad \ldots(8)$$

When D is a matrix with the dimensions M by N, U and V are unitary matrices with the dimensions M by M and N by N, respectively, whose nonzero norm by the diagonal components is equal to the singular values of H. Thus, Equation (1) may be expressed as follows:

$$Y = UDV^H x + N \quad \ldots(9)$$

1.3.From MIMO to mm MIMO

Massive MIMO, in combination with other technologies such as as small cells, (HetNets) and (mm wave) technology, is positioned to play a remarkable role in the development of 5G networks, which are now working to deal with the issues given by the transmission rate bubble. The previously mentioned options are seen as prospective solutions to enhance this existing pattern further. Considerable MIMO research has shown that just increasing the number of transmitter antennas enables constantly obtaining a greater SNR whilst maintaining perfect channel state information and completely removing pilot contamination. Cellular densification is an additional effect of massive MIMO. Similar to Cooper's law, the increase in capacity will mostly result from the deployment of more dense cells. The expanding challenges faced by massive MIMO technology include concerns related to energy efficiency and the provision of low latency backhauls, which are crucial for facilitating higher transmission rates, amongst several other factors [19-21].

1.4. Free space propagation model

The assumption that underpins the model of propagation in free space is that the surrounding environment is clear of any interference or impediments. Thus, elements such as reflection, refraction and other effects of a similar kind are not accounted for in this model. Whilst communication occurs between entities, the use of the omnidirectional antenna wave transmission model may be employed to account for power attenuation between the transmitter and receiver. This outcome can be accomplished by using the relevant equation given by [7].

$$\frac{p_r}{p_t} = \left[\frac{\sqrt{G}}{4\pi d}\lambda\right] \quad \ldots(10)$$

In the context of free space transmission, the variables Pr, Pt, G, λ and d represent the received power, transmitted power, product of the transmitter and receiver antenna field radiation patterns, wavelength, and distance between the transmitter and receiver, respectively [11]. Free-space path loss (FSPL) refers to the reduction in signal strength or attenuation of radio energy between the feed points of two antennas. FSPL is computed using Equation (10); the equation of FSPL is given by [5].

$$\text{FSPL} = 20\log_{10}(d) + 20\log_{10}\left(\frac{4\pi}{c}\right) \quad \ldots(11)$$

where the operational frequency starts at f = 28 GHz, and the distance between the transmitter and receiver is d = (100–300 m). The two PL models for better comparability are also considered. The close in free space (CI FS) reference distance PL model is first considered. Equation (1) provides the expression for the CI FSPL model. The equation of PLCI is given by [5].

$$(f, d)[dB] = \text{plfs}(f, d_0)[dB] + 10\, n \log_{10}\left(\frac{d}{d_0}\right) \quad \ldots(12)$$

where n is the PL exponent, and (f, d_0) is the FS PL for an isotropic antenna at a distance of = 1 m [17]. Thus, Equation (13) can be derived by [5], as follows:

$$pl^{CI}(f, d)[dB] = \text{plfs}(f, 1)[dB] + 10\, n \log_{10}(d)$$

... (13)

The loss of FS propagation at a distance = 1 m equation now becomes, given by [5].

$$\text{plfs}(f, 1\text{m})[\text{dB}] = 20\log_{10}\left(\frac{4\pi f}{c}\right) \quad \ldots (14)$$

where C denotes light's speed. The final equation of the CI model, which is given by Equations (13) and (14) as follows by [5]

$$\text{pl}^{\text{CI}}(f,d)[\text{db}] = 20\log_{10}\left(\frac{4\pi f}{c}\right) 10\ n \log_{10}\left(\frac{d}{d_0}\right) \quad \ldots (15)$$

The equation of PL CI model can be represented by [11]:

$$\text{PL}^{\text{CI}}(f, d)\ [\text{dB}] = \text{FSPL}(f, d_0)[\text{dB}] + 10n \log_{10}\left(\frac{d}{d_0}\right) + \chi_{\sigma}^{\text{CI}}, \text{ where } d \geq d_0 \quad \ldots (16)$$

where n is the path loss exponent (PLE), χCI is the CI FS reference distance, and f is also expressed in gigahertz (for the CI). With a standard deviation measured in dB, σ represents a zero-mean Gaussian random variable. To determine the mean PL with distance and frequency, the CI model employs two parameters (the PLE n and $\chi_{\sigma}^{\text{CI}}$), whereas the ABG model requires three parameters. A helpful feature of Equation (16) is that starting at d0, 10n expresses route loss in dB as a function of decades of distances, which makes mentally computing power over distance when d_0 is set to 1 m extremely simple [11]. In (16), the carrier frequency is represented by the symbol f, and the FSPL at a T-R distance to separation of d0 in dB is indicated by the symbol FSPL (f, d_0); the equation is given by [11].

$$\text{FSPL}(f, d_0)[\text{dB}] = 20\log_{10}\left(\frac{4\pi f d_0 \times 10^9}{c}\right) \quad \ldots (17)$$

The CI model may be expressed as follows by [11]:

$$\begin{aligned}\text{PL}^{\text{CI}}(f, d)[\text{dB}] &= \text{FSPL}(f, d_0)[\text{dB}] + 10n\log_{10}(d/d_0) + \chi_{\sigma}^{\text{CI}} \\ &= 10n\log_{10}\left(\frac{d}{d_0}\right) + 20\log_{10}\left(\frac{4\pi d_0 \times 10^9}{c}\right) \\ &\quad + 20\log_{10}(f) + \chi_{\sigma}^{\text{CI}} \\ &= 10n\log_{10}\left(\frac{d}{d_0}\right) + \eta + 20\log_{10}(f) + \chi_{\sigma}^{\text{CI}},\end{aligned}$$

$$\text{where } d \geq d_0, \eta = 20\log_{10}\left(\frac{4\pi d_0 \times 10^9}{c}\right) \quad \ldots (18)$$

$$\chi_{\sigma}^{\text{CI}} = \text{PL}^{\text{CI}}(f, d)[\text{dB}] - \text{FSPL}(f, 1\text{ m})[\text{dB}] - 10n\log_{10}(d) = A - nD \quad \ldots (19)$$

where A represents the difference between PLCI (f, d)[dB] and FSPL(f, 1m)[dB], whereas D represents 10 log10(d). Then, the SF standard deviation is

$$\sigma^{\text{CI}} = \sqrt{\frac{\sum \chi_{\sigma}^{\text{Cl}\ 2}}{N}} = \sqrt{\frac{\sum (A - nD)^2}{N}} \quad \ldots (20)$$

where N stands for the number of PL data points.

This paper shows that for indoor and outdoor channels throughout a broad spectrum of microwave- and millimeter-wave frequencies, the CI FS standard distance d0 = 1 m yields excellent parameter stability and model accuracy, as well develops a consistent modeling technique. Setting a standard measure of 1 m for the near field of large antenna arrays reduces inaccuracy in wireless system design and is more achievable than the ABG model given in [11]. The ABG model is the second PL model. Equation (16) by [11] provides the equation for the ABG model.

$$\text{PL}^{\text{ABG}}(f, d)[\text{dB}] = 10\alpha \log_{10}\left(\frac{d}{1\text{ m}}\right) + \beta + 10\gamma \log_{10}\left(\frac{f}{1\text{GHz}}\right) + \chi_{\sigma}^{\text{ABG}} \quad \ldots (21)$$

B = PL^{ABG}(f, d)[dB], D = 10 log10(d) and F = 10 log10(f) from (19) are used, and the SF is given by[11]

$$\chi_{\sigma}^{\text{ABG}} = B - \alpha D - \beta - \gamma F. \quad \ldots (22)$$

The SF standard deviation

$$\sigma^{\text{ABG}} = \sqrt{\frac{\sum \chi_{\sigma}^{\text{ABG}^2}}{N}} = \sqrt{\frac{\sum (B - \alpha D - \beta - \gamma F)^2}{N}} \quad \ldots (23)$$

The notation (f, d) [dB] describes the PL at a certain frequency (f) and distance (d). This notation is used to signify the coefficients that indicate the dependency of PL on distance and frequency. Similarly, the optimal compensation value for PL in dB may be represented, where d indicates the distance between the transmitter and receiver, and f denotes the carrier frequency in gigahertz (GHz). To establish line-of-sight communication inside an urban environment, the parameters α, β and are carefully chosen. The values of the parameters are shown in the following bracket.

$$\begin{cases} \propto = 1 \\ \beta = 69.4 \\ \gamma = 2 \end{cases}$$

For simulations, the distance, d, between the transmitter and receiver is set at 100 m, and the frequency, f, is set at (28–60) GHz. The CI model in Equation (15) contains a single parameter and a frequency dependency of PL. The frequency-dependent FSPL term is the main way to represent its frequency dependency.

The ABG models' three parameters, namely, alpha, beta and gamma, depend on several factors in addition to frequency (Equation 16) [22-26].

The CI model's frequency dependency is mainly indicated by the frequency-dependent FSPL component in the initial meter of free-space

propagation, whereas the ABG and CI models with d0 = 1 m are functions of range and frequency. In the indoor office situation, recent data reveal that the PL rises with frequency throughout the mm wave range (the β and γ parameters are used for curve fitting). When the ABG model includes an enhancement parameter β and a frequency weighting term γ, which lack an established scientific basis, it departs from physics. A reference distance of 1 m is used to calculate the term in the ABG model.

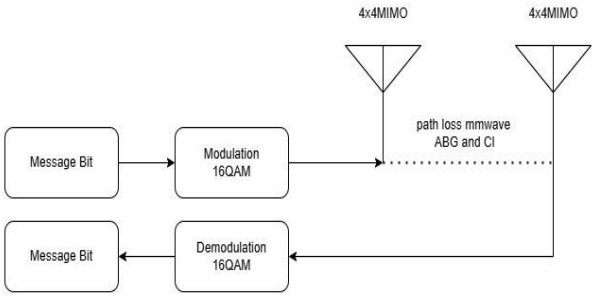

Fig. 1. Proposed 4×4 MIMO system model for BER reduction utilising PL models

2. Proposed System Model

To increase bit error rate (BER), two PL models (ABG and CI) are utilised between the transmitter and reception antenna. The proposed system model is illustrated in Figure 1. It is based on a W-OFDM system rather than a normal OFDM system. First, bits of stream are utilised as an input and transmit only one binary bit of information. The next stage involves modulating a high-frequency carrier signal with digital information. Demodulation, or the opposite of modulation, occurs at the receiving end. Two modulation schemes (16-QAM and 16-PSK) are employed. Two types of PL models (ABG and CI) are utilised between the transmitter and reception antennas to reduce BER. The suggested system model is displayed in Figure 1.

3. Results and Descussion

Table 1,
Parameters of the Simulated Model in Brief

Matlab Version	**2022a**
Message Typ	**12800 binary bits**
Operating frequency (f)	GHz 28 GHz 60
Carrier spacing	kHz 60
Data rate	Mbps 48
Bandwidth	MHz 20
Antenna configuration	4×4
D0	1 m
IFFT / FFT	Size 256

Table 2,
Parameters in the CI path loss model (Δ^{σ} discrepancy in the standard deviation of sf between the CI and CI at d_0 = 10)

LOS (Line of sight)						
Frequency range (GHz)	**Distance (m)**	**Model**	**Path loss exponent (PLE)**	**d0 (m)**	**σ (dB)**	**Δ σ**
28	100–300	CI model	2	1m	1,3	0
28	100–300	CI model	2	10 m	1,3	-
38	100–300	CI model	2,1	1m	1,4	0,1
38	100–300	CI model	2,1	10m	1,3	-
48	100–300	CI model	2,1	1m	1,1	0,1
48	100–300	CI model	2,1	10m	1	-
60	100–300	CI model	2	1m	0.6	0
60	100–300	CI model	2	10m	0,6	-

Table 3,
Parameters in the ABG path loss model (Δ^{σ} difference in the standard deviation sf between the ABG and ABG at d_0 = 10)

LOS (Line of sight)								
Frequency range (GHz)	**Distance (m)**	**Model**	**α**	**β**	**γ**	**d0 (m)**	**σ (dB)**	Δ σ
28	300–100	ABG Model	1	69,4	2	1**m**	4	0
28	300–100	ABG Model	1	69,4	2	10**m**	4	-
38	300–100	ABG Model	1	69,4	2	1**m**	4	0
38	300–100	ABG Model	1	69,4	2	10m	4	-
48	300–100	ABG Model	1	69,4	2	1**m**	4	0
48	300–100	ABG Model	1	69,4	2	10**m**	4	-
60	300–100	ABG Model	1	69,4	2	1**m**	3.9	0
60	300–100	ABG Model	1	69,4	2	10m	3.9	-

Table 4,
Parameters in the CI and the ABG path loss models (Δσ difference in the standard deviation sf between the CI and ABG at d0 = 10)

NLOS (Nonline of sight)										
Frequency range in (GHz)	**Distance (m)**	**Model**	**Path loss exponent (PLE)**	**α (ABG)**	**β (ABG)**	**γ (ABG)**	**$d_0$in meter**	**(dB) for σ CI model**	**(dB) σ for ABG model**	**=(σ Δ (dB) σ CI-(dB)for σ ABG)**
28	300	CI model	2	1	69.4	2	10m	4.1		0.1
28	300	ABG Model	-	1	69.4	2	10m	-	4	-
38	300	CI model	2	1	69.4	2	10m	4.9		0.2
38	300	ABG Model	-	1	69.4	2	10m	-	4.7	-
48	300	CI model	2	1	69.4	2	10m	4.9		0
48	300	ABG Model	-	1	69.4	2	10m	-	4.7	-
60	300	CI model	2.1	1	69,4	2	10m	5		0.1
60	300	ABG Model	-	1	69,4	2	10m	-	4.7	-

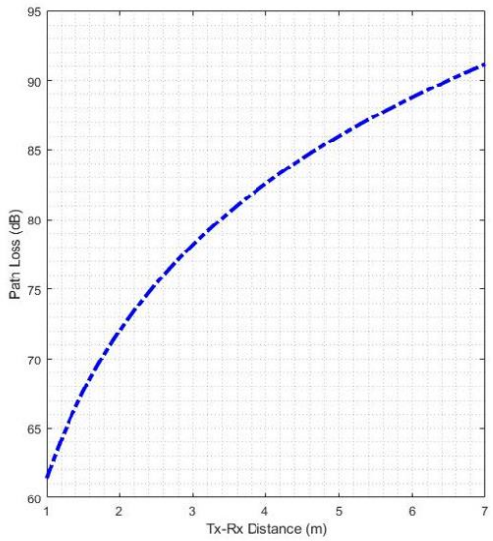

Fig. 2. CI PL model for the 4×4 MIMO at 28 GHZ frequencies and complex indoor room scenario

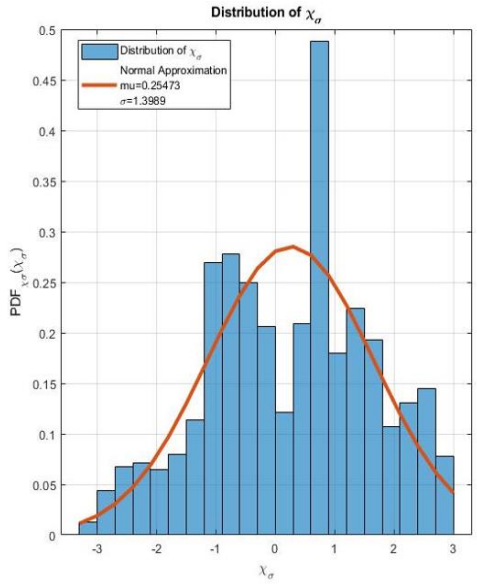

Fig. 3. Normal distribution of PL model for the 4×4 MIMO at 28 GHZ frequencies and complex indoor room scenario

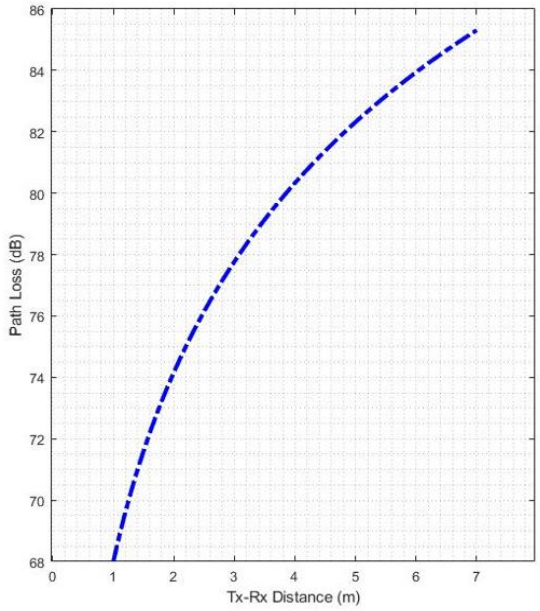

Fig. 4. CI PL model for the 4×4 MIMO at 60 GHZ frequencies and complex indoor room scenario

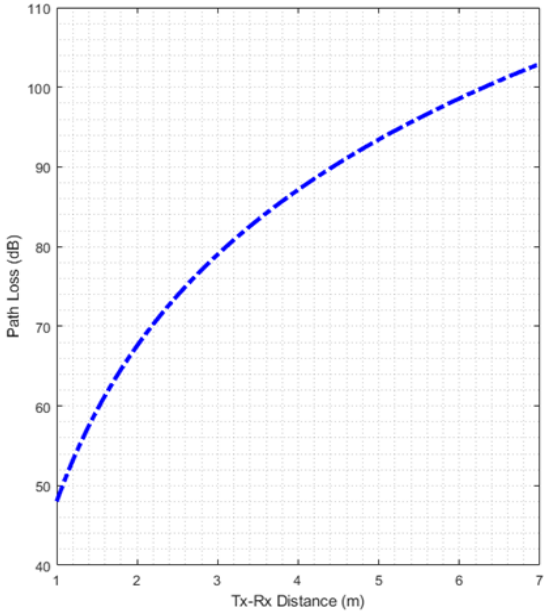

Fig. 6. ABG PL model for the 4×4 MIMO at 28 GHZ frequencies and complex indoor room scenario

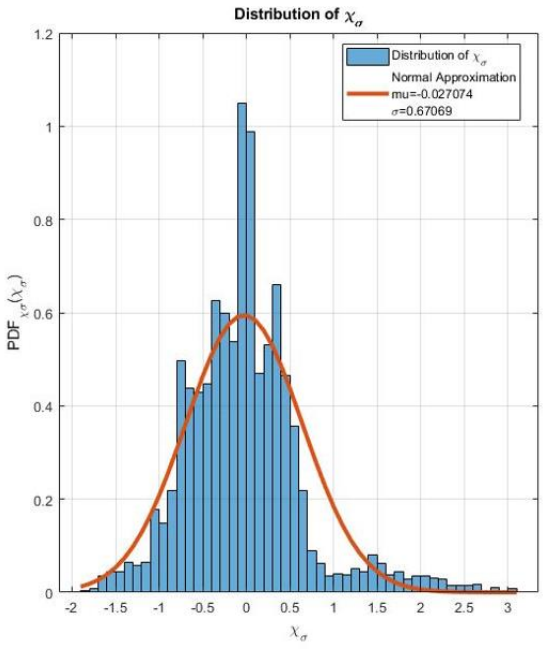

Fig. 5. Normal distribution of PL model for the 4×4 MIMO at 60 GHZ frequencies and complex indoor room scenario

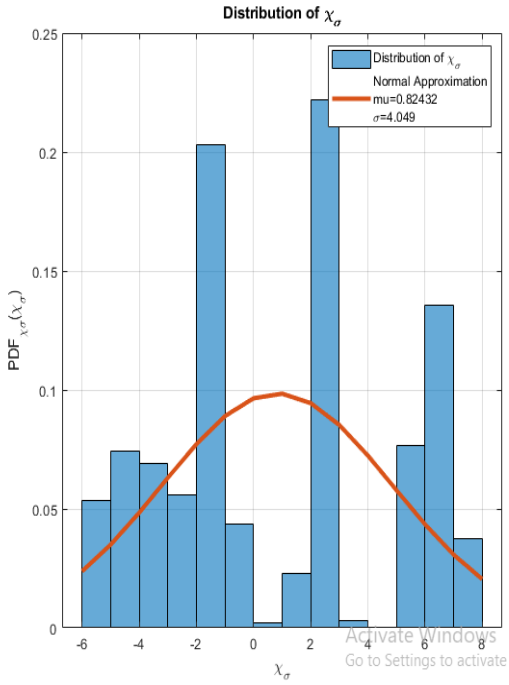

Fig. 7. Normal distribution of PL model for the 4× 4 MIMO at 28 GHZ frequencies and complex indoor room scenario

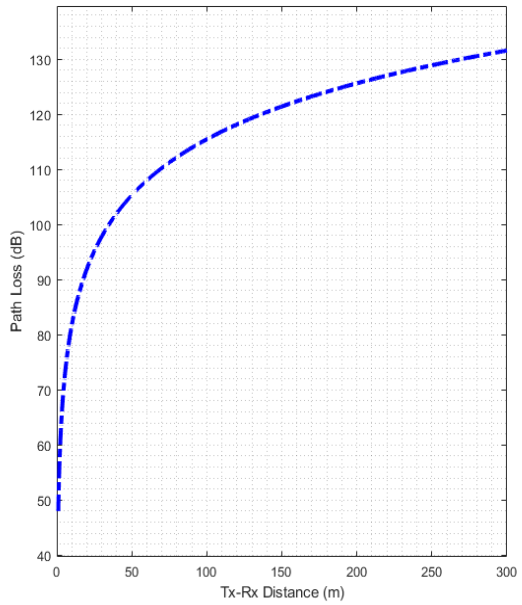

Fig. 8. ABG PL model for the 4×4 MIMO at 60 GHZ frequencies and complex indoor room scenario

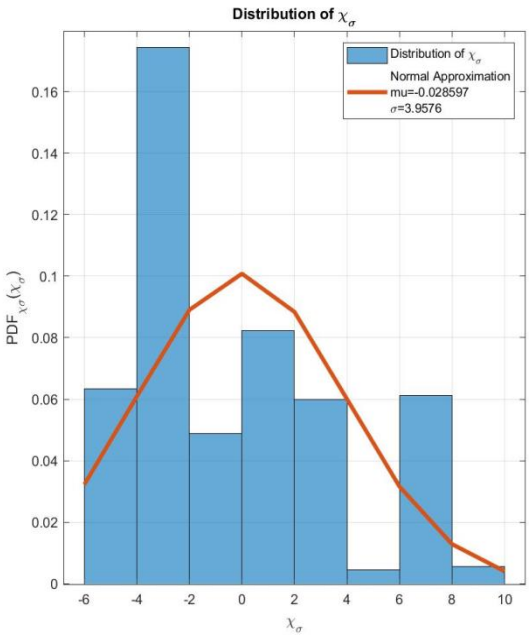

Fig. 9. Normal distribution of PL model for the 4×4 MIMO at 60 GHZ frequencies and complex indoor room scenario

4. Conclusion

This paper uses collections of measured data from 28 GHz to 60 GHz to examine and contrast two large-scale propagation route loss models, namely, ABG (three elements) and the CI (two elements), over the mm wave frequency ranges. Initially, the 1 m CI model and the CI model with a reference distance = 10 are compared. The two-parameter 1 m CI model yields about equal accuracy. The results demonstrate that on the one hand, in the presence of data sets, the prediction accuracies of the ABG and CI models are extremely comparable despite the ABG model's need for additional model parameters and absence of a physical foundation for its floating-intercept value. On the other hand, the CI model is physically connected to the transmitter power by using a 1-meter CI FS reference distance, which has a built-in frequency dependency over the whole mm wave range. In contrast to the physically based CI with fewer model parameters, the ABG model has parameter values that vary substantially over various distances and frequencies whilst typically only slightly lowering the SF standard deviation. A collection of data points is given, and the single largest difference between the standard deviations for two models across all situations is (2.7) dB for the mm wave range. Nevertheless, a more recent research [12] using a considerably larger data set reveals a mere 0.4 dB difference in an outdoor case. This paper demonstrates using a 28 GHz for example how the ABG NLOS model is naturally inaccurate at short and long (several hundred m) distances. It also underestimates interference at long distances when applied at an arbitrary frequency in comparison to CI and predicts less than free space loss when near the TX. Thus, capacity simulations generated by the ABG model are extremely optimistic. The simulation findings between the ABG and CI models differ considerably, particularly with regard to planned small-cell deployments where interference might be produced by hundreds of nearby BSs. The paper's key contribution is a sensitivity analysis that demonstrates that the CI model outperforms the others in terms of stability and prediction accuracy (i.e. SF standard deviation) over a wide range of frequencies. The CI model performs than the ABG model when applied to forecasting PL at various distances and frequencies compared with the data set used to identify the PL models' parameters. Therefore, the sensitivity analysis in this paper demonstrates that the CI model is more robust, accurate and reliable compared with the ABG model for unforeseen circumstances or instances when a route loss model may be applied to varying distances or frequencies that differ from the data used to develop the original model. Finally, using the measured PL as an example in outdoor environments demonstrates a low degree of dependency on frequency within the first meter of

free-space propagation (which is represented by the FSPL term). The CI model is the best fit for outdoor environments due to its accuracy and ease of use. The actual CI FS reference point of this device contributes to its excellent sensitivity performance levels .

References

[1] J. G. Andrews, F. Baccelli, and R. K. Ganti, "A tractable approach to coverage and rate in cellular networks," IEEE Transactions on communications, vol. 59, no. 11, pp. 3122-3134, 2011.

[2] M. Di Renzo, C. Merola, A. Guidotti, F. Santucci, and G. E. Corazza, "Error performance of multi-antenna receivers in a Poisson field of interferers: A stochastic geometry approach," IEEE Transactions on Communications, vol. 61, no. 5, pp. 2025-2047, 2013.

[3] M. Di Renzo, A. Guidotti, and G. E. Corazza, "Average rate of downlink heterogeneous cellular networks over generalized fading channels: A stochastic geometry approach," IEEE Transactions on Communications, vol. 61, no. 7, pp. 3050-3071, 2013.

[4] M. Di Renzo and W. Lu, "The equivalent-in-distribution (EiD)-based approach: On the analysis of cellular networks using stochastic geometry," IEEE Communications Letters, vol. 18, no. 5, pp. 761-764, 2014.

[5] M. H. Mahmud, K. Khaleduzzaman, S. Sarker, and L. C. Paul, "Effect of Path Loss Models on Performance of 5G Compatible MIMO WINDOW-OFDM Systems," in 2020 International Conference on Smart Technologies in Computing, Electrical and Electronics (ICSTCEE), 2020: IEEE, pp. 257-262.

[6] F. Di Stasio, M. Mondin, and F. Daneshgaran, "Multirate 5G downlink performance comparison for f-OFDM and w-OFDM schemes with different numerologies," in 2018 international symposium on networks, computers and communications (ISNCC), 2018: IEEE, pp. 1-6.

[7] J. Park, H.-B. Jeon, J. Cho, and C.-B. Chae, "Measurement-based Close-in Path Loss Modeling with Diffraction for Rural Long-distance Communications," IEEE Wireless Communications Letters, 2023.

[8] M. K. Elmezughi and T. J. Afullo, "Investigations into the effect of high-ordering the log-distance dependency of path loss models for indoor wireless channels," International Journal on Communications Antenna and Propagation, vol. 12, no. 1, pp. 1-12, 2022.

[9] M. Di Renzo, "Stochastic geometry modeling and analysis of multi-tier millimeter wave cellular networks," IEEE Transactions on Wireless Communications, vol. 14, no. 9, pp. 5038-5057, 2015.

[10] T. S. Rappaport, S. Sun, and M. Shafi, "5G channel model with improved accuracy and efficiency in mmWave bands," IEEE 5G Tech Focus, vol. 1, no. 1, pp. 1-6, 2017.

[11] S. Sun et al., "Investigation of prediction accuracy, sensitivity, and parameter stability of large-scale propagation path loss models for 5G wireless communications," IEEE transactions on vehicular technology, vol. 65, no. 5, pp. 2843-2860, 2016.

[12] L. Lu, G. Y. Li, A. L. Swindlehurst, A. Ashikhmin and R. Zhang, "An Overview of Massive MIMO: Benefits and Challenges," in IEEE Journal of Selected Topics in Signal Processing, vol. 8, no. 5, pp. 742-758, Oct. 2014.

[13] [13] N. A. Muhammad, P. Wang, Y. Li, and B. Vucetic, "Analytical model for outdoor millimeter wave channels using geometry-based stochastic approach," IEEE Transactions on Vehicular Technology, vol. 66, no. 2, pp. 912-926, 2016.

[14] [14] A. A. Budalal and M. R. Islam, "Path loss models for outdoor environment—with a focus on rain attenuation impact on short-range millimeter-wave links," e-Prime-Advances in Electrical Engineering, Electronics and Energy, vol. 3, p. 100106, 2023.

[15] [15] S. F. Nawaf, "Channel Capacity Improvement of MIMO Communication Systems using Different Techniques," Tikrit Journal of Engineering Sciences, vol. 25, no. 1, pp. 36-41, 2018

[16] J. Lu, and H. b. Zhu, "Stochastic multiple-input multiple-output channel model based on singular value decomposition," IET Communications, vol. 9, no. 15, pp. 1852-1856, 2015.

[17] O. O. Erunkulu, A. M. Zungeru, C. K. Lebekwe, and J. M. Chuma, "Cellular communications coverage prediction techniques: A survey and comparison," IEEE Access, vol. 8, pp. 113052-113077, 2020.

[18] W. Lu and M. Di Renzo, "Stochastic geometry modeling and system-level analysis & optimization of relay-aided downlink cellular networks," IEEE Transactions on

Communications, vol. 63, no. 11, pp. 4063-4085, 2015.

[19] T. Bai, R. Vaze, and R. W. Heath, "Analysis of blockage effects on urban cellular networks," IEEE Transactions on Wireless Communications, vol. 13, no. 9, pp. 5070-5083, 2014.

[20] S. Sun, G. R. MacCartney, and T. S. Rappaport, "A novel millimeter-wave channel simulator and applications for 5G wireless communications," in 2017 IEEE international conference on communications (ICC), 2017: IEEE, pp. 1-7.

[21] M. J. da Silva, D. C. Begazo, and D. Z. Rodríguez, "Evaluation of speech quality degradation due to atmospheric phenomena," in 2019 International Conference on Software, Telecommunications and Computer Networks (SoftCOM), 2019: IEEE, pp. 1-6.

[22] L. F. Abdulameer, U. Sripati, and M. Kulkarni, "BER Performance Improvement of Dual Chaotic Maps Based on STBC Communication System," Al-Khwarizmi Engineering Journal, vol. 18, no. 4, pp. 32-44, 2022.

[23] M. Shafi et al., "Microwave vs. millimeter-wave propagation channels: Key differences and impact on 5G cellular systems," IEEE Communications Magazine, vol. 56, no. 12, pp. 14-20, 2018.

[24] A. A. H. Budalal, M. R. Islam, K. Abdullah, and T. A. Rahman, "Modification of distance factor in rain attenuation prediction for short-range millimeter-wave links," IEEE Antennas and Wireless Propagation Letters, vol. 19, no. 6, pp. 1027-1031, 2020.

[25] Z. A. Shamsan, "Rainfall and diffraction modeling for millimeter-wave wireless fixed systems," IEEE Access, vol. 8, pp. 212961-212978, 2020.

[26] A. A. Budalal, I. M. Rafiqul, M. H. Habaebi, and T. A. Rahman, "The effects of rain fade on millimetre wave channel in tropical climate," Bulletin of Electrical Engineering and Informatics, vol. 8, no. 2, pp. 653-664, 2019.

[27] I. Shayea, T. Abd. Rahman, M. Hadri Azmi, and A. Arsad, "Rain attenuation of millimetre wave above 10 GHz for terrestrial links in tropical regions," Transactions on emerging telecommunications technologies, vol. 29, no. 8, p. e3450, 2018.

نماذج فقدان المسار لنظام الاتصالات اللاسلكية الجيل الخامس باستخدام قناة اتصال الموجات الملمترية

زينة اسامة داود
قسم هندسة المعلومات والاتصالات، كلية الهندسة الخوارزمي، جامعة بغداد، بغداد، العراق
البريد الالكتروني: zina_osama@kecbu.uobaghdad.edu.iq

المستخلص

يمكن لطوبولوجيا هوائي MIMO (متعددة المدخلات والمخرجات المتعددة) في أنظمة الاتصالات اللاسلكية زيادة سعة القناة والموثوقية. يعد استخدام نطاقات تردد الموجات المليمترية جنبا إلى جنب مع التقنيات الأخرى خطوة مهمة في تحقيق معدلات بيانات عالية للوسائط المتعددة المتطورة وأجهزة الذكاء الاصطناعي. ومع ذلك ، فإن إرسال إشارات تردد الموجة المليمترية يواجه تحديات مثل التلاشي وتأخير الوقت والانتشار وفقدان التشتت. وبالتالي ، فإن تحسين معلمات الانتشار أمر بالغ الأهمية لتحسين الأداء. تبحث هذه الدراسة في تأثير نماذج فقدان المسار تبحث هذه الدراسة في تأثير نماذج فقدان المسار (PL) (ABG و CI) على تصميم وتحليل نظام MIMO W-OFDM 4×4 باستخدام تقنية التشكيل QAM-16 للاتصالات اللاسلكية من الجيل الخامس. تفحص الورقة البحثية أنظمة MIMO W-OFDM باستخدام نموذجيCI PL و ABG PL لتقييم فقدان المسار بالديسيبل والتوزيع الطبيعي والانحراف المعياري. ووفقًا لنتائج المحاكاة، فإن نظام MIMO W-OFDM القائم على نموذج CI PL مع التشكيل الرقمي QAM-16 مرن للغاية وفعال في استرجاع الإشارات المرسلة.